

**NJC**

**The Influence of Copper Addition on Electrical Conductivity  
and Charge Transfer Resistance of Reduced Graphene Oxide  
(rGO)**

Journal:	<i>New Journal of Chemistry</i>
Manuscript ID	NJ-ART-07-2018-003614.R1
Article Type:	Paper
Date Submitted by the Author:	20-Aug-2018
Complete List of Authors:	Iskandar, Ferry; Institute of Technology Bandung, Physics; Abdillah, Oktaviardi; Institut Teknologi Bandung, Department of Physics Stavila, Erythrina; Research Center for Nanosciences and Nanotechnology (RCNN), Institut Teknologi Bandung, Jl. Ganesha 10 Bandung, 40132, Indonesia, Aimon, Akfiny; Department of Physics, Faculty of Mathematics and Natural Sciences , Institut Teknologi Bandung, Jl. Ganesha 10 Bandung, 40132, Indonesia.

SCHOLARONE™  
Manuscripts



## ARTICLE

## The Influence of Copper Addition on Electrical Conductivity and Charge Transfer Resistance of Reduced Graphene Oxide (rGO)

Ferry Iskandar,<sup>\*a,b,c</sup> Oktaviardi Bityasmawan Abdillah,<sup>a</sup> Erythrina Stavila,<sup>c</sup> and Akfiny Hasdi Aimon<sup>a,b</sup>

Received 00th January 20xx,  
Accepted 00th January 20xx

DOI: 10.1039/x0xx00000x

www.rsc.org/

The electrical conductivity and charge transfer resistance ( $R_{ct}$ ) of reduced graphene oxide (rGO) with the addition of copper are reported. The samples of rGO with copper addition were successfully synthesized via in situ chemical exfoliation using a microwave-assisted technique. Annealing was performed at various temperatures to determine the optimal annealing temperature for the sample with the best electrical conductivity performance. The resulting samples were characterized using attenuated total reflectance-Fourier transform infrared (ATR-FTIR) characterization, X-ray diffraction (XRD), Raman spectrometry, energy dispersive X-ray (EDX) spectrometry, scanning electron microscopy (SEM), four-point probe, and electrochemical impedance spectroscopy (EIS). The highest conductivity value of 24.85 S/cm was obtained for the rGO sample with addition of 1 wt% copper treated with annealing at 300 °C for 45 minutes. The electrochemical properties of the samples were characterized using electrochemical impedance spectroscopy (EIS), resulting in a charge transfer resistance ( $R_{ct}$ ) value of 3.86  $\Omega$  for sample **B** with the addition of 1 wt% copper. The possible reaction mechanism and explanations on the influence of Cu, Cu<sub>2</sub>O, and CuO on the electrical and charge transfer resistance value of the rGO are also described in this report.

### Introduction

The discovery of graphene has had a massive impact on scientific research development. Graphene is an allotrope of carbon that consists of a sp<sup>2</sup> carbon atom planar monolayer with a hexagonal structure resembling a honeycomb.<sup>1-3</sup> In 2004,<sup>2</sup> Geim and Novoselov first introduced a graphene isolation technique and since then more methods have been developed for producing graphene. Nowadays, synthesis of graphene can be accomplished through various synthetic techniques, such as chemical vapor deposition, exfoliation (including oxidation and reduction), epitaxial growth, and chemical synthesis.<sup>3,4</sup> The oxidation and reduction method is a preferred synthetic route due to its low cost and its ability to be applied in large-scale production. This method involves three steps, beginning with graphite oxidation, exfoliation of the graphite oxide to graphene oxide (GO), followed by reduction to produce reduced graphene oxide (rGO).

Graphene is known to have a large surface area (2630 m<sup>2</sup>g<sup>-1</sup>), high electron mobility ( $\sim 2 \times 10^5$  cm<sup>2</sup>V<sup>-1</sup>s<sup>-1</sup>), excellent electrical ( $\sim 2000$  S/cm) and high thermal ( $\sim 5000$  Wm<sup>-1</sup>K<sup>-1</sup>) conductivity properties.<sup>5,6</sup> Due to these extraordinary properties, graphene is used in various applications, especially in electronic devices, such as energy storage devices,<sup>4, 6-8</sup> biosensors,<sup>9, 10</sup> optoelectronic devices,<sup>3</sup> transistors,<sup>11</sup> and transparent conductors.<sup>3</sup>

Synthesis of graphene via oxidation and reduction methods results in reduced graphene oxide (rGO). In rGO, some oxygen-containing functional groups remain in the graphene sheets, which causes defects in the graphene crystal. These defects lead to interruption of the electron mobility, resulting in lower electrical conductivity.<sup>6</sup> To overcome this issue, rGO or GO synthesis techniques with the addition of various metals, metal oxides, and semiconducting and magnetic nanomaterials have been developed to improve the electrical and electrochemical properties of rGO.<sup>4, 6</sup> Moreover, by adding these materials to synthesize composites with rGO, they can also act as spacers between rGO sheets to hinder agglomerations caused by Van der Waals interactions between the rGO sheets.<sup>1,4</sup>

Copper is the metal that has the second highest electrical conductivity (5.96  $\times 10^7$  S/m at 20 °C) after silver. Compared to silver, copper is more frequently used in electronic applications because of its high abundance and relative inexpensiveness. Moreover, copper has a high boiling point, which makes it useful for fabrication involving high-temperature and high-pressure chemical reactions, such as microwave-assisted reactions, vapor phase reactions, and

<sup>a</sup> Department of Physics, Faculty of Mathematics and Natural Sciences, Institut Teknologi Bandung, Jl. Ganesha 10 Bandung, 40132, Indonesia. E-mail: ferry@fi.itb.ac.id.

<sup>b</sup> National Center for Sustainable Transportation Technology (NCSTT), Institut Teknologi Bandung, Jl. Ganesha 10 Bandung, 40132, Indonesia.

<sup>c</sup> Research Center for Nanosciences and Nanotechnology (RCNN), Institut Teknologi Bandung, Jl. Ganesha 10, Bandung, 40132, Indonesia.

† Electronic Supplementary Information (ESI) available: table listing the XRD parameters for the various rGO samples, the Raman spectra of the GO, SEM pictures of rGO/Cu/Cu<sub>2</sub>O E, the distribution curve for rGO/Cu/Cu<sub>2</sub>O E, and the possible mechanism of further reduction of rGO with annealing treatment. See DOI: 10.1039/x0xx00000x.

various organic transformations.<sup>12</sup> Due to its excellent properties, copper and its metal oxides (CuO and Cu<sub>2</sub>O) are actively used as components for preparing nanocomposites with rGO, for example Cu<sub>2</sub>O/CuO/rGO as biosensor electrode for ascorbic acid detection,<sup>13</sup> CuO/graphene for high-performance lithium storage,<sup>14</sup> Cu-rGO as catalyst electrode toward non-enzymatic glucose oxidation reactions,<sup>15</sup> Mn<sub>1-x</sub>Cu<sub>x</sub>Fe<sub>2</sub>O<sub>4</sub>/rGO<sup>7</sup> and rGO/Cu<sub>2</sub>O/Cu as electrodes in supercapacitors.<sup>16</sup>

Synthesis of graphene in the presence of nanoparticles (including metal or metal oxide) can be performed via two methods, i.e. post immobilization (ex situ hybridization) and in situ binding (in situ crystallization).<sup>17</sup> Ex situ hybridization is performed by mixing a solution of graphene and pre-synthesized nanoparticles, which have been surface-functionalized prior to mixing the nanoparticles and graphene sheets. The composites resulting from this method may exhibit low density and non-uniform nanostructure coverage of the graphene sheets.<sup>17</sup> Therefore, we used the in situ binding method, being a simple and straightforward method. This method involves simultaneous reduction of graphene oxide (GO) and CuO using hydrazine as the reducing agent under microwave-assisted irradiation.

Microwave-assisted synthesis of graphene-based composites has been performed previously. Various metal and metal oxides, including Cu,<sup>15</sup> CuO and Cu<sub>2</sub>O,<sup>13</sup> Bi<sub>8</sub>La<sub>10</sub>O<sub>27</sub>,<sup>18</sup> CuS,<sup>19</sup> Fe<sub>2</sub>O<sub>3</sub>,<sup>20</sup> TiO<sub>2</sub>,<sup>21</sup> Ag,<sup>22-24</sup> ZnO, (CoMn)<sub>3</sub>O<sub>4</sub>,<sup>25</sup> LiFePO<sub>4</sub>,<sup>26</sup> AgZnFe<sub>2</sub>O<sub>4</sub>,<sup>27</sup> CoMoO<sub>4</sub>,<sup>28</sup> have been successfully used for producing graphene-based composites using microwave-assisted synthesis. However, in this report, we synthesized rGO/Cu/Cu<sub>2</sub>O from the simultaneous reduction of GO and CuO solution using a microwave-assisted method. Microwave-assisted synthesis of rGO/Cu has been successfully performed by Hsieh *et al.*,<sup>15</sup> who used a Cu<sup>2+</sup> concentration of 10, 20, 30 wt%. Their study focused on the electrochemical properties of rGO/Cu and the catalytic performance of Cu in rGO sheets for non-enzymatic glucose oxidation.<sup>15</sup> The result on non-enzymatic glucose oxidation reported by Luo *et al.* shows the electrochemical performance of rGO/Cu.<sup>10</sup> A composite of rGO/Cu<sub>2</sub>O/Cu has been synthesized using a hydrothermal method for the reduction of GO solution and Cu foil.<sup>16</sup> A composite of rGO/Cu<sub>2</sub>O/Cu was characterized for application as supercapacitor, so the electrochemical properties of rGO/Cu<sub>2</sub>O/Cu were thoroughly reported.<sup>16</sup> However, these investigations of rGO/Cu and rGO/Cu<sub>2</sub>O/Cu<sup>10, 15, 16</sup> focused on their electrochemical properties and further applications. Therefore, no study has been conducted yet that focuses on the electrical conductivity properties of rGO with copper addition and the influence of Cu, Cu<sub>2</sub>O, and CuO on electron transport with rGO sheets.

In this research, we studied the influence of Cu, CuO, and Cu<sub>2</sub>O on the electrical conductivity and charge transfer resistance ( $R_{ct}$ ) of the resulted samples. We studied how the presence of Cu, CuO, and Cu<sub>2</sub>O influences the electrical conductivity and electrochemical properties of rGO. We synthesized rGO and rGO with copper addition via in situ chemical exfoliation using a microwave-assisted method.

Previously, our group has successfully performed microwave-assisted synthesis of rGO.<sup>29, 30</sup> In the present study, we used the same rGO synthesis method as reported previously;<sup>30</sup> the only difference was that we added cupric oxide (CuO) as a copper precursor for synthesizing rGO with copper addition during the reduction process. In a previously reported preparation of rGO/Cu<sub>2</sub>O/Cu, a high concentration of copper precursor ( $\geq 10$  wt%) was used.<sup>15</sup> However, in this study, low concentrations of copper precursor (0.5, 1, 2, 3, and 5 wt%) were used, employing the appropriate amount of GO and CuO solution so we could determine the effect of copper addition on the electrical conductivity of the materials. We also investigated the annealing treatment of the rGO samples with the addition of copper under various annealing temperatures and times in order to determine which conditions could improve the electrical conductivity of the resulting samples.

## Materials and methods

**Materials.** Graphite flakes, concentrated sulfuric acid (H<sub>2</sub>SO<sub>4</sub>, 98%), potassium permanganate (KMnO<sub>4</sub>), ethylene glycol, phosphoric acid (H<sub>3</sub>PO<sub>4</sub>), copper sulfate (CuSO<sub>4</sub>), and hydrazine solution (80% in water) (N<sub>2</sub>H<sub>4</sub>) were purchased from Merck. Hydrochloric acid (HCl), deionized water, and ethanol were acquired from Smartlab Indonesia. Sodium hydroxyl (NaOH) and hydrogen peroxide (H<sub>2</sub>O<sub>2</sub>) were obtained from Bratachem.

### Synthesis of reduced graphene oxide (rGO) with the addition of copper.

CuSO<sub>4</sub> powder (5 g) was diluted in 10 mL DI water, and subsequently 0.04 mole of NaOH was added until precipitation of Cu(OH)<sub>2</sub> was formed. The precipitate of Cu(OH)<sub>2</sub> was washed three times with DI water and then with alcohol 70%, respectively. Next, the precipitate of Cu(OH)<sub>2</sub> was dried in an oven at 60 °C for 12 h. After the sample had dried, the reduction process was carried out by heating the Cu(OH)<sub>2</sub> powder at 700 °C for 3 h, which resulted in black powder CuO. In the synthesis of rGO/Cu/Cu<sub>2</sub>O, a certain amount of CuO powder was used. Percent weight variations of CuO (0.5, 1, 2, 3, and 5%) compared to graphite oxide (1 gram from mixture of CuO and graphite oxide) were prepared with the solution concentration maintained at 0.1 M. The CuO powders were dispersed in ethylene glycol by stirring and subsequently sonicated for 25 minutes until a homogeneous solution was achieved.

Graphite oxide was synthesized using the same method reported previously by our group.<sup>30</sup> Graphene oxide suspensions (GO) were prepared by dispersing graphite oxide into ethylene glycol (EG). Dispersing was conducted by ultraturrax and subsequent exfoliation was done by sonication for 2 h. Later, the CuO solution was added to the GO suspensions, followed by sonication for 25 minutes.

The reduction process to synthesize rGO with the addition of copper precursor was carried out as follows. Reduction was carried out by adding 1 mL hydrazine (N<sub>2</sub>H<sub>4</sub>) to the rGO and CuO mixture solution. The reduction process of GO and CuO

was completed by treating the mixture solution with microwave irradiation (Panasonic Microwave 2.45 MHz, 800 W) in low mode for 20 minutes. Then, the reaction mixture was centrifuged. The residue was washed three times with deionized water and subsequently washed three times using alcohol 70%. The sample was poured into a petri dish and dried for 12 h at 60 °C. The dried samples were further characterized. The rGO samples with the addition of copper synthesized with different percent weights of Cu (0.5, 1, 2, 3, and 5 wt%) in the mixture of CuO and GO during the reduction process were labeled as sample A, sample B, sample C, sample D, and sample E, respectively. We also synthesized rGO using the same procedure as mentioned above but without the addition of copper precursor. This rGO was used as reference for further characterizations and was labeled rGO.

**Instrumental methods.** The resulting samples of rGO and rGO with the addition of copper were characterized using the following instrumental methods. Attenuated total reflectance-Fourier transform infrared (ATR-FTIR) spectrometry measurements were carried out using Alpha FTIR Spectrometer Bruker 1 176 397. X-ray diffraction (XRD) measurements were performed on a Phillips Analytical PW 1710 BASED diffractometer. Raman spectrometry measurements were carried out by using a Horiba Jobin Yvon Modular Raman spectrometer with laser excitation wavelength at 514 nm (green) and a Stellar Pro Argon-ion laser with laser power at 50 mW. Electrical conductivity properties were measured by a four-point probe, which involved four electrodes from one electrical source (Advantest R6240A DC Voltage) and a Keithley multimeter. Before the electrical conductivity measurements, the samples were pelleted by lab hot press equipment, but without heat treatment, and subsequently annealed for 30 minutes. Different annealing temperatures (100, 200, 300, 400, and 500 °C) at standard atmospheric condition were applied. The aim of the use of various annealing temperatures was to determine the influence of temperature on the electrical conductivity of the samples. After the optimal temperature in the annealing process was determined, an investigation on the effect of annealing time on electrical conductivity was performed by applying various annealing times (15, 30, 45, and 60 minutes) to the samples at the optimal annealing temperature. Scanning electron microscopy (SEM) was done using an SEM SU3500 instrument at 15 kV. Energy dispersive X-ray (EDX) spectrometry measurements were performed using a JEOL-JSN-6510LV instrument. Electrochemical impedance spectroscopy (EIS) was carried out with a Gamry 3000 instrument, using  $\text{Hg}_2\text{Cl}_2$  as the reference electrode, Pt as the auxiliary electrode, and rGO or rGO with copper addition as the working electrode.

## Results and discussion

### Structural analysis of rGO and rGO with the copper addition

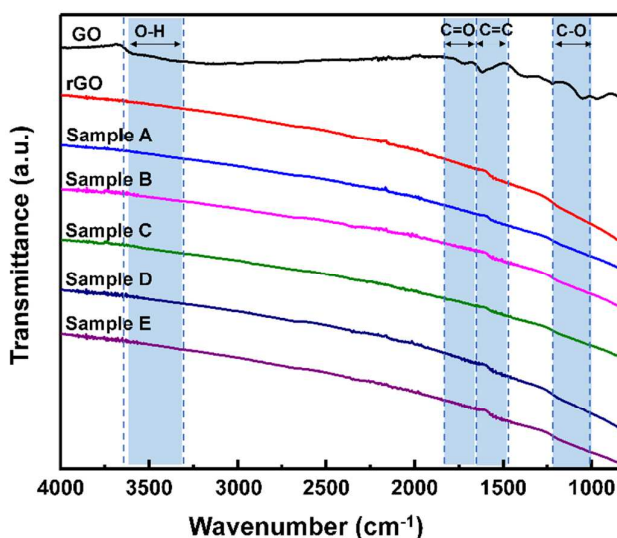


Fig. 1 ATR-FTIR spectra of graphene oxide (GO), reduced graphene oxide (rGO), and samples A-E.

Functional group identification was carried out by analyzing the ATR-FTIR measurement results. The ATR-FTIR spectra of the GO, rGO, and samples of rGO with copper addition are depicted in Fig. 1. From the graphene oxide spectrum, the characteristic peaks correlated to oxygen-containing functional groups (including the peak at 2700-3300  $\text{cm}^{-1}$  belonging to O-H, the peak at 1600-1800  $\text{cm}^{-1}$  belonging to C=O, and the peak at 1000-1300  $\text{cm}^{-1}$  belonging to C-O) could be identified, which means oxidation of graphite was performed successfully. After reduction of the graphene oxide, these characteristics of the oxygen-containing functional groups no longer existed (see Fig. 1), which proved the successful removal of oxygen-containing groups during the reduction process. However, the peak at 1600  $\text{cm}^{-1}$  corresponding to C=C aromatic group still appeared since it belongs to the  $\text{sp}^2$  carbon structure of the graphene layer.<sup>29, 31</sup>

From the ATR-FTIR spectra, we could not distinguish the difference between the rGO sample and the rGO samples with the addition of copper; thus, XRD measurements of the rGO samples with the addition of copper had to be performed. XRD diffractograms of the GO, rGO, and samples A-E are shown in Fig. 2. Details of the average crystallites sizes ( $D$ ) and the interlayer spacing ( $d$ ) of all samples, i.e. GO, rGO, and rGO with copper addition (A-E), can be found in Table S1 in the Supplementary Information. By comparing the XRD diffractograms of the GO and the rGO, we could confirm that the reduction of GO to rGO had been successfully performed. The XRD diffractogram of the GO shows the characteristic peak plane (0 0 2) of GO at  $2\theta = 9.68^\circ$  with a broad  $d$ -spacing value of 0.912 nm. The  $d$ -spacing value represents the spacing between the layers in the graphene. After reduction of the GO, the peak plane (0 0 2) shifted to a higher  $2\theta$  value at  $24.16^\circ$  with a lower  $d$ -spacing value of 0.368 nm, as visible in the XRD diffractogram of rGO in Fig. 2. The diffraction peak at  $2\theta = 24.16^\circ$  is recognized as a characteristic graphene peak belonging to the (002) plane of the hexagonal graphite

structure.<sup>14</sup> The lower *d*-shifting value after the reduction process resulted from the removal of the oxygen-containing functional groups that intercalate in between the layers of graphene.<sup>29</sup> The interlayer spacing (*d*) values of the rGO samples with the addition of copper (A-E) displayed a similar value as the rGO, as can be seen in Table S1 in the Supplementary Information.† Moreover, the diffraction peak

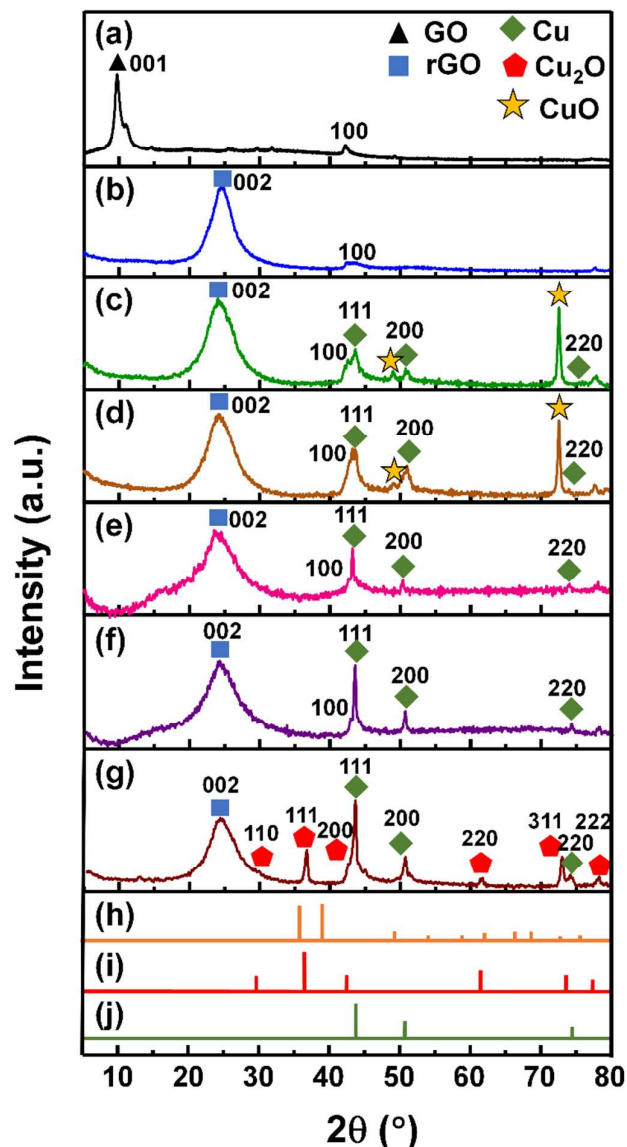


Fig. 2 XRD diffractogram of (a) GO, (b) rGO, (c) sample A, (d) sample B, (e) sample C, (f) sample D, and (g) sample E, (h) CuO (JCPDS-45-0937), (i), Cu<sub>2</sub>O (JCPDS-05-0667), and (j) Cu (JCPDS-04-0836).

plane (1 0 0) at  $2\theta = 42^\circ$  can be attributed to the short-range order in the graphene layers.<sup>32</sup>

Fig. 2(c-g) shows diffraction peaks that indicate the presence of rGO and Cu phases. In samples A-E, the diffraction peaks at  $2\theta$  of  $43^\circ$  and  $50^\circ$  correlate to Cu crystal. The diffraction peaks at  $43^\circ$  and  $50^\circ$  indicate face-centered cubic Cu crystal with orientations (1 1 1) and (2 2 0), which is in

agreement with JCPDS card no. 04-0836.<sup>33</sup> These results confirm the presence of Cu crystal in samples A-E.

The diffractograms of samples A and B are shown in Fig. 2(c-d). Characteristic diffraction peaks belonging to CuO crystal were observed from these diffractograms. The diffraction peaks at  $2\theta$  of  $49^\circ$  and  $72^\circ$  represent CuO crystal with orientation (-2 0 2) and (3 1 1), which is in agreement with JCPDS card no. 45-0937.<sup>34</sup> Moreover, the diffraction peak at  $2\theta$  of  $\sim 77^\circ$  indicates the presence of Cu<sub>2</sub>O phase. A similar diffraction peak belonging to Cu<sub>2</sub>O can be observed in the diffractograms of samples C and D, see Fig. 2(e-f). No diffraction peaks from CuO crystals are visible; there are only peaks from rGO, Cu, and Cu<sub>2</sub>O crystals. In the diffractogram of sample E, Fig. 2(g) there are diffraction peaks at  $2\theta$  of  $36^\circ$ ,  $42^\circ$ ,  $61^\circ$ ,  $73^\circ$ , and  $77^\circ$ , which can be attributed to Cu<sub>2</sub>O phases, which is in line with JCPDS card no. 05-0667.<sup>13</sup> Furthermore, a diffracting peak representing the presence of CuO was observed in this sample.

Based on the XRD analysis results, the reaction mechanism during the reduction of graphene oxide and CuO is proposed as shown in Fig. 3. By varying the addition of copper in the synthesis, there are three possible reaction mechanisms. For samples A and B, the first possible reaction follows the path in Fig. 3(a). In the initial part of the reduction, see reaction path (i), hydrazine performs the reduction of GO and CuO resulting in rGO and Cu. Due to the relatively low amount of CuO in the reaction mixture, the hydrazine is able to convert all Cu<sup>2+</sup> to Cu. Since the reduction process still transpires, the presence of Cu may also play a role as a reducing agent in the reaction. A previously reported result showed that Cu can be used as GO reducing agent.<sup>35</sup> Thus, the next reaction takes path (ii), which shows further reduction of rGO and oxidation of Cu to Cu<sup>+</sup> and Cu<sup>+</sup> by Cu as reducing agent. The final products are rGO, CuO, Cu<sub>2</sub>O, and the remaining Cu.

Fig. 3(b) shows the possible reaction mechanism for samples C and D. The addition of copper concentration of 2 and 3 wt% to the reaction mixture of GO and CuO follows the reduction reaction in path (iii). By using these respective concentrations, the hydrazine is able to perform the reduction reaction for GO to rGO and reduces all Cu<sup>2+</sup> to Cu with Cu<sup>+</sup> as a side product.

In Fig. 3(c), path (iv) shows the possibility of a reduction reaction when we used 5 wt% copper concentration in the reaction mixture of GO and CuO. The resulted product from this reduction process contains rGO, Cu, Cu<sup>+</sup>, and remaining Cu<sup>2+</sup>. The CuO and Cu<sub>2</sub>O resulted from the uncompleted reduction of CuO to Cu because more CuO was added in the synthesis process but the hydrazine remained the same

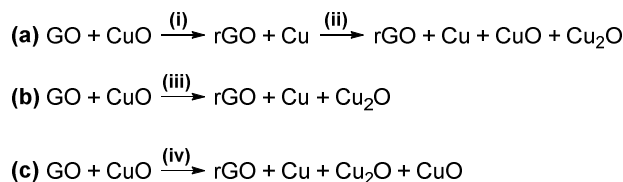


Fig. 3 Possible mechanism reduction reactions using hydrazine as reducing agent between GO and CuO when the concentration of copper in the reaction mixture are (a) 0.5 and 1 wt%, (b) 2 and 3 wt%, and (c) 5 wt%.

amount in all variations, which means that there was not enough hydrazine to perform the reduction of  $\text{Cu}^{2+}$  to Cu.

Further structural characterization of sample **B** was performed using Raman spectroscopy. The Raman spectrum of the rGO was used as a reference. There are three characteristics of graphene in the Raman spectrum, i.e. the D peak at  $\sim 1350\text{ cm}^{-1}$  from  $\text{sp}^3$  carbon atoms from defects (the D peak is absent in high-quality graphene), the G peak at  $\sim 1580\text{ cm}^{-1}$  correlating to  $\text{sp}^2$  carbon atoms, and an intense 2D (also known as  $\text{G}'$ ) peak at  $\sim 2700\text{ cm}^{-1}$  corresponding to the second-order mode of the D band.<sup>36</sup> Fig. 4(a) shows the Raman spectra of the rGO and sample **B**. In the Raman spectrum of the rGO, peaks were observed at  $1354\text{ cm}^{-1}$  (D band),  $1576\text{ cm}^{-1}$  (G band) and  $2683\text{ cm}^{-1}$  (2D band). Likewise, three peaks were identified at  $1354\text{ cm}^{-1}$  (D band),  $1580\text{ cm}^{-1}$  (G band) and  $2682\text{ cm}^{-1}$  (2D band) in the Raman spectrum of sample **B**. There is also a peak at  $\sim 2900\text{ cm}^{-1}$  (D+G band), which represents disorder due to combination scattering.<sup>37</sup> The D/G peak area ratio results for the rGO and sample **B** were 1.09 and 1.13, respectively. This ratio of the D and G band ( $I_D/I_G$ ) represents an estimation of the disorder level in the graphene.<sup>38</sup> Sample **B** had higher  $I_D/I_G$  compared to the rGO, which means a higher disorder level due to the presence of copper and oxygen-containing functional groups remaining in the graphene sheets. Moreover, Fig S1 in the Supplementary Information shows the intensity ratio of the D and G band ( $I_D/I_G$ ) of sample GO (0.81), rGO (1.09), and sample **B** (1.13). These  $I_D/I_G$  values represent the disorder level in the graphene. The increase of the  $I_D/I_G$  value can be attributed to the decrease in the average size of the  $\text{sp}^2$  hybridization domain after the reduction process. As previously reported, reduction of GO results in a restoration of the  $\text{sp}^2$  hybridization in the graphitic domain. This leads to a

smaller  $\text{sp}^2$  hybridization domain compared to GO.<sup>39, 40</sup> Meanwhile, the higher  $I_D/I_G$  value of sample **B** compared to that of the rGO sample was due to the higher disorder level in sample **B**, which resulted from the presence of Cu and more remaining oxygen-functional groups.

Apart from the ratio between the D band and the G band, there is the ratio between the 2D band and the G band ( $I_{2D}/I_G$ ), which corresponds to the presence of metal doping in the graphene.<sup>41</sup> In Fig. 4(a), the  $I_{2D}/I_G$  in sample **B** (0.66) was lower compared to the  $I_{2D}/I_G$  in the rGO (0.68). This result is in line with a previously reported result, which showed that the presence of metal in graphene results in a decrease of  $I_{2D}/I_G$ .<sup>41</sup> Moreover, the inset of Fig. 4(b) and (c) displays the G and 2D bands, respectively. In Fig. 4(b), splitting of the G band of sample **B** can be observed. The G band shifted from  $1576.9\text{ cm}^{-1}$  (rGO) to  $1580.9\text{ cm}^{-1}$  and  $1609.3\text{ cm}^{-1}$ . This upshift and splitting of the G band and slight downshift of the 2D band (see Fig. 4(c)) represent n-doping interaction between the metal and the graphene.<sup>41, 42</sup> From the 2D band profile, we conclude that the resulted rGO and sample **B** were both multilayers. This result is based on the previously reported results that showed multilayers graphene has a broad 2D peak and a wavenumber higher than  $2673\text{ cm}^{-1}$ .<sup>43</sup>

#### Morphological analysis of rGO and rGO with the copper addition

The morphology of the samples was characterized by SEM, EDX and element mapping measurement. An SEM image, the EDX and the mapping results of sample **B** are shown in Fig. 5. Fig. 5(a) displays the graphene sheets resulted from the exfoliation process. The SEM image also shows small particle on the graphene layer surface, see Fig. 5(a). Further EDX measurement was performed to confirm the existence of copper in sample **B** (see Fig. 5(b)). The EDX result showed a small amount of copper, which is in agreement with the small amount copper used in the synthesis of sample **B** (1 wt% of copper in the mixture of  $\text{CuO}$  and GO). The further mapping of the EDX results is shown in Fig. 5(c-f). In Fig. 5(f), the copper was slightly concentrated in a particular area and probably belonged to the small particle on top of the graphene sheet. However, the copper was also distributed quite nicely on the rGO surface.

SEM pictures of the rGO and all rGO samples with copper addition can be found in Fig. S2 (a-e) in the Supplementary Information.† The SEM images of the rGO samples with copper addition were compared to the SEM image of the rGO. The average particle sizes of Cu,  $\text{Cu}_2\text{O}$ , and  $\text{CuO}$  in samples **A-E** were 515, 483, 568, 579, and 647 nm, respectively. These calculated average particle sizes of Cu,  $\text{Cu}_2\text{O}$ , and  $\text{CuO}$  show an increasing tendency in average particle size with the increase of the concentration of copper precursor. However, the average particles sizes of Cu,  $\text{Cu}_2\text{O}$ , and  $\text{CuO}$  in sample **A** were bigger than in sample **B**. This happened because of particle agglomeration in sample **A**.

More copper (Cu,  $\text{Cu}_2\text{O}$ , and  $\text{CuO}$ ) particles were observed on the graphene sheet surface of sample **E** than on sample **B**, as can be seen in Fig. S3 (a) in the Supplementary

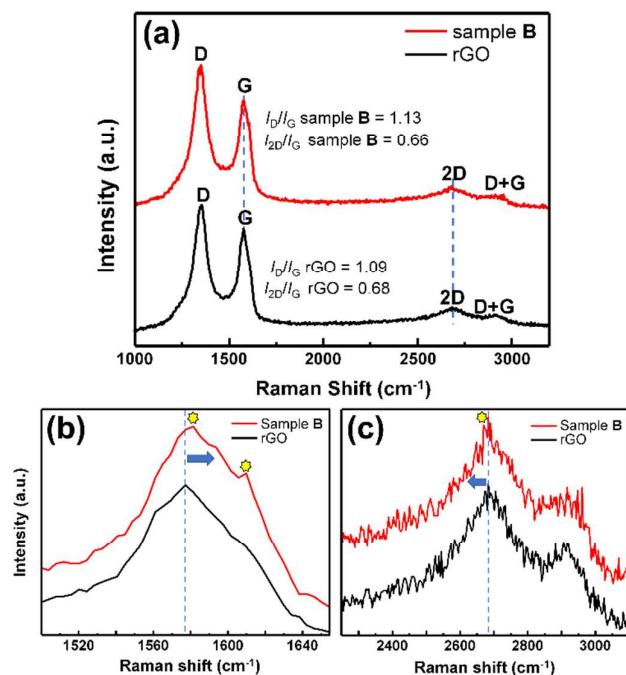


Fig. 4 (a) Raman spectra of rGO and sample **B**, (b) inset Raman spectra of G band, and (c) inset Raman spectra of 2D band.

Information.† In the synthesis of sample E, a higher amount of copper was added compared to sample B. This resulted in more copper and Cu<sub>2</sub>O particles in sample E than in sample B. Copper, Cu<sub>2</sub>O, and CuO particles were also found on the edges

of the graphene sheet, as shown in Fig. S3 (b) in the Supplementary Information.†

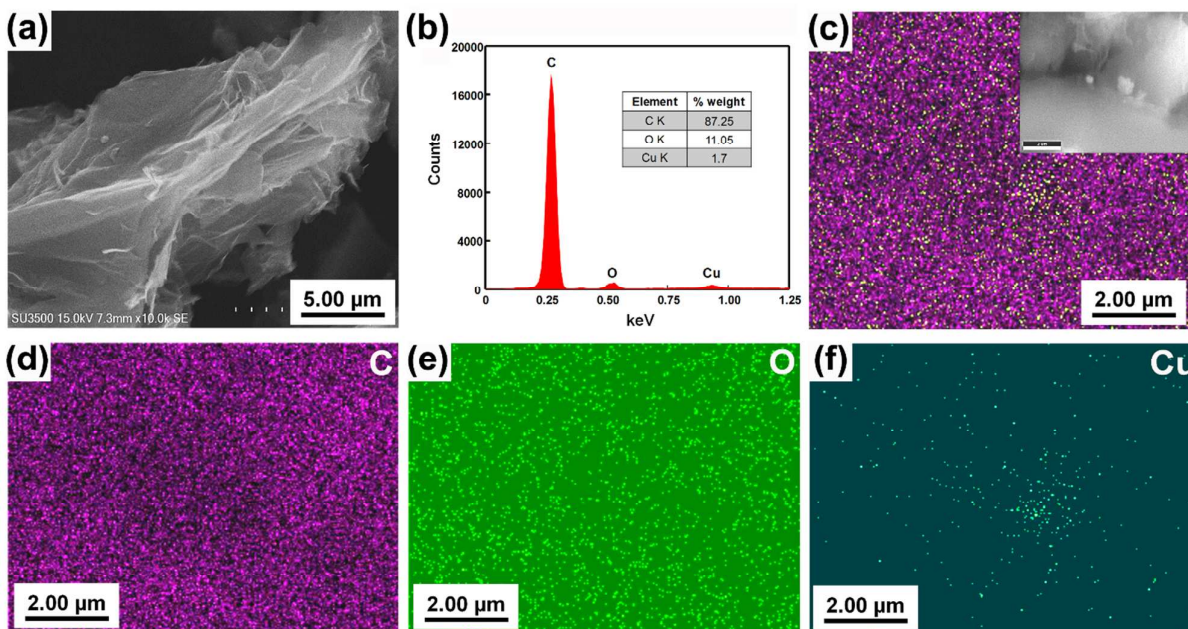


Fig. 5 (a) SEM picture, (b) EDX result, and (c) entire mapping of sample B, (d) mapping from carbon (C), (e) mapping from oxygen (O), and (f) mapping from copper (Cu) in the sample B.

The summary of the EDX results in Table 1 further confirms the successful reduction of the GO. Detailed information on the EDX results of the GO, rGO, and rGO samples with copper addition can be found in Fig. S4-S9 in the Supplementary Information.† The reduction of the oxygen-containing functional groups from GO is indicated by the increase of the carbon to oxygen ratio (C/O) from 1.73 (GO) to 7.28 (rGO). A higher C/O ratio value indicates better removal of oxygen-containing functional groups from GO. By increasing the addition of copper precursor in the synthesis, the amounts of formed Cu<sub>2</sub>O and of remaining CuO in the sample were increased. The Cu/O ratio values increased with the increase of the copper precursor added in the synthesis. Moreover, Table 1 also shows that the %wt of the Cu in the rGO samples with copper addition determined using EDX resulted in a relatively similar amount compared to the initial amount of copper precursor added in the synthesis.

Table 1 EDX results for rGO and samples of rGO with the copper addition

Samples	Elements in the sample (wt%)			Element Ratio		
	C	O	Cu	C/O	C/Cu	Cu/O
GO	63.38	36.62	-	1.73	-	-
rGO	87.92	12.08	-	7.28	-	-
Sample A	86.12	13.16	0.72	6.54	119.61	0.05
Sample B	87.25	11.05	1.70	7.90	51.32	0.15

Sample C	84.16	13.93	1.92	6.04	43.83	0.14
Sample D	84.57	12.02	3.41	7.04	24.80	0.28
Sample E	83.89	10.37	5.75	8.09	14.59	0.55

#### Electrical conductivity of rGO and rGO with the copper addition

Electrical conductivity characterization was performed to determine the electron mobility of the rGO samples with addition of copper. By comparing the electrical conductivity of the rGO sample and the rGO samples with copper addition, we determined the influence of the addition of a small amount of copper on the electron mobility of the samples, which is shown in Fig. 6(a) and (b). The effect of the annealing temperature on the electrical conductivity is displayed in Fig. 6(a). By introducing annealing treatment at 100, 200, and 300 °C, the conductivity of the rGO samples with copper addition increased with the increase in annealing temperature. However, when the annealing temperature was increased up to 400 °C, the samples of rGO with copper addition showed a decrease in electrical conductivity. By applying the annealing treatment at 500 °C, the pellet form of the rGO samples with copper addition was destroyed. Thus, there were no pellets for electrical conductivity measurements. Different results were obtained from the rGO. The electrical conductivity of the rGO increased with the increase of the annealing temperature up to 400 °C. The pellet form of the rGO was still preserved with annealing treatment at 500 °C. Thus, by adding copper, the

thermal stability of the rGO was reduced. The presence of copper in rGO might interrupt the Van de Waals interaction between the graphene sheets and consequently decrease the thermal stability. From these results, we can conclude that the highest electrical conductivity was observed for the samples treated with annealing treatment at 300 °C.

Fig. 6(b) shows the influence of the copper concentration on the electrical conductivity of the samples. These electrical conductivity results are from the samples treated with annealing at 300 °C for 30 minutes. The addition of 0.5 and 1 wt% copper increased the electrical conductivity of the samples. On the other hand, when the addition of the copper concentration increased (2, 3, and 5 wt%), the electrical conductivity of the samples decreased. This happened because of the presence of more Cu<sub>2</sub>O and remaining CuO in the sample. From the reported results of Valladares *et al.*, copper oxides (CuO and Cu<sub>2</sub>O) have a high electrical resistivity.<sup>44</sup> Hence, the existence of Cu<sub>2</sub>O and CuO in the samples led to a decrease in electrical conductivity of the rGO with the addition

of copper at a concentration of 2, 3, and 5 wt%. However, Cu<sub>2</sub>O and CuO were also present in samples A and B. Because of less copper added in the synthesis (0.5 and 1 wt%, respectively), there was less Cu<sub>2</sub>O and CuO. Moreover, from the proposed mechanism reaction, in sample A and B, reduction of rGO also occurred because the presence of Cu may act as reducing agent. However, in sample A, we observed agglomerations of Cu, Cu<sub>2</sub>O, and CuO particles. Similar agglomerations were observed in samples C, D, and E. Therefore, sample B displayed the highest electrical conductivity among all samples.

Furthermore, the C/O ratio values from the EDX results correlated with the conductivity of the samples. The higher the C/O ratio value, the better the removal of the oxygen-containing functional groups in GO. With better removal of the oxygen-containing functional groups, the resulted product is expected to have better electrical conductivity properties. By comparing the C/O ratio values of the rGO sample and samples A-E, the highest C/O ratio value of 8.09 was observed for sample E. However, the highest conductivity was shown by sample B. Therefore, the EDX results confirmed that the presence of Cu<sub>2</sub>O and CuO decreases the electrical conductivity of rGO.

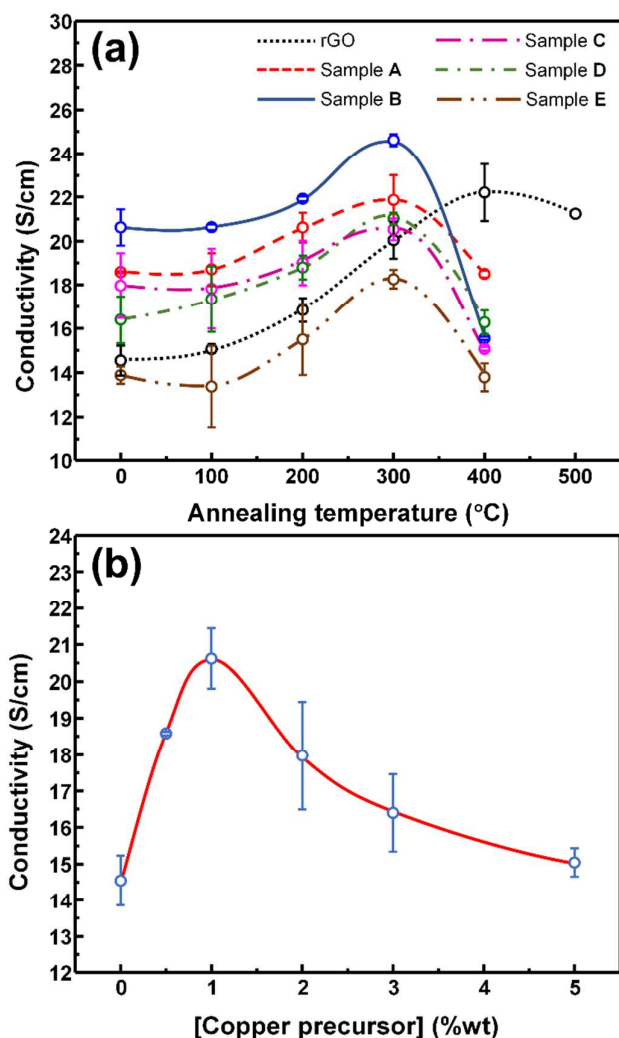


Fig. 6 (a) Influence of various annealing temperatures on electrical conductivity results of rGO and rGO with the addition of copper and (b) effect of the addition of copper precursor in rGO on the electrical conductivity after treated with annealing process at 300 °C for 30 min.

As shown in Fig. 6, the annealing treatment increased the electrical conductivity of the rGO sample and the rGO samples with copper addition. By applying annealing, a further reduction of the rGO sample may take place, as shown in Fig. S10 in the Supplementary Information.† The possible mechanism reaction was proposed based on the previously reported mechanism reaction,<sup>45</sup> where heating the rGO at high temperature resulted in further removal of oxygen-containing functional groups (–COOH and –OH), producing CO<sub>2</sub> and CO as the product of the reduction process. To some extent, this annealing treatment increases the electrical conductivity because the removal of oxygen-containing functional groups produces more sp<sup>2</sup> carbon structure, and thus improves the electron mobility in the graphene sheet. However, applying a too extended annealing treatment results in a decrease in electrical conductivity. As shown in the possible mechanism reaction, the removal of –OH groups produces CO and leads to a vacancy in the graphene sheet.<sup>29</sup> This vacancy disrupts the sp<sup>2</sup> carbon structure and consequently results in a decrease of electrical conductivity, see Fig. 7. By applying annealing at 300 °C for ≤ 45 minutes (15, 30, and 45 minutes), the conductivity

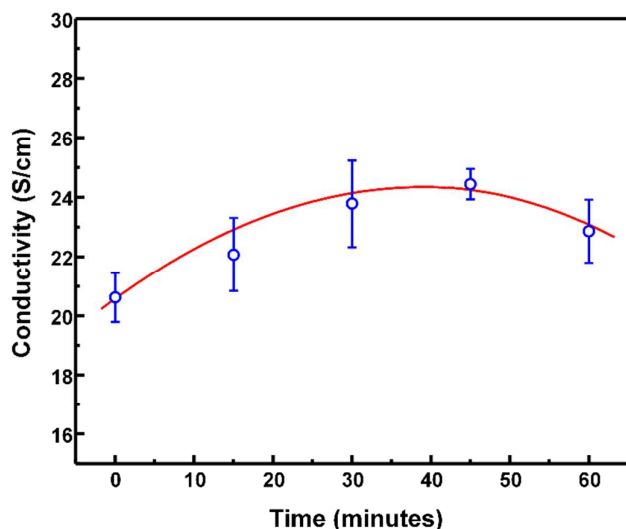


Fig. 7 Influence of the annealing time on the conductivity results of sample B.

of sample B increased, and more than 45 minutes annealing at 300 °C resulted in a decrease of the conductivity of the sample. The highest conductivity of 24.85 S/cm resulted from annealing at 300 °C for 45 minutes.

Furthermore, the temperature during the reduction process under microwave conditions was examined per each minute of the reaction, as shown in Fig. S11 in the Supplementary Information.† Fig. S11 represents the temperature profile in function of reaction time under microwave conditions. The highest reaction temperature of 168 °C was observed after 19 minutes reaction time. As previously reported by Larciprete *et al.*, the removal of oxygen-containing functional groups such as CO<sub>2</sub> can be achieved at a temperature of 350-450 K (77-177 °C).<sup>46</sup> Therefore, the mechanism reaction shown in Fig. S10 is a

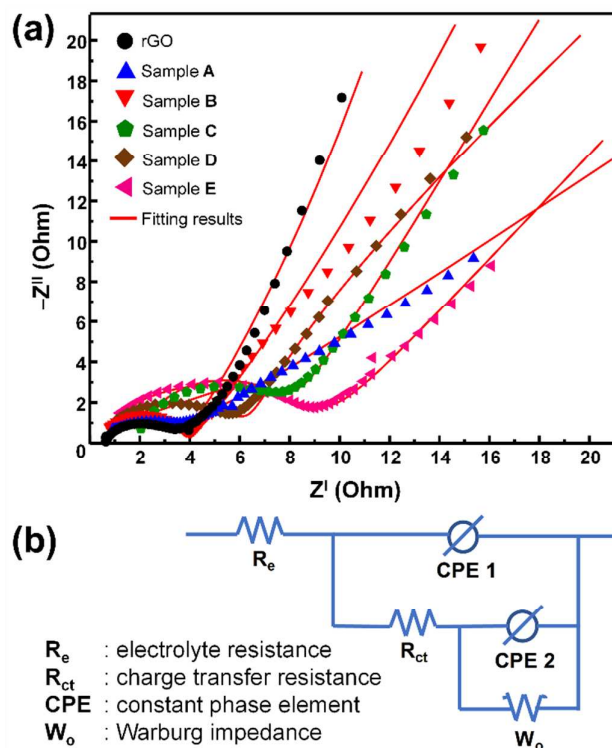


Fig. 8 (a) Nyquist curves of rGO and samples A-E and (b) model of the equivalent electrical circuit.

possible mechanism reaction not only for heating during annealing but also during heating under microwave conditions.

#### Charge transfer resistance ( $R_{ct}$ ) values of rGO and rGO with the copper addition

The electrochemical properties of the samples were characterized by EIS measurement. EIS measurement produces data consisting of information of real (x-axis) and imaginary (y-axis) impedance, as shown in Fig. 8(a). The equivalent electrical circuit used as the model circuit is shown in Fig. 8(b). The charge transfer resistance ( $R_{ct}$ ) value is equal to the semicircle diameter from the Nyquist curve. The  $R_{ct}$  values from the samples of rGO and rGO with the addition of copper are listed in Table 2. The goodness of fit value is a parameter that corresponds to the fitting error. The goodness of fit values range from 10<sup>-4</sup>-10<sup>-2</sup>, indicating a fitting error < 10%.<sup>47</sup> In Table 2, the rGO had the lowest  $R_{ct}$  value (3.30 Ohm) compared to the other samples. Examining only the samples of rGO with the addition of copper, sample B had a smaller  $R_{ct}$  of 3.86 Ohm compared to the other samples with copper addition. The  $R_{ct}$  value of sample B showed a value close to the  $R_{ct}$  value of the rGO, which indicates a similar ability in electron transport. Moreover, the previously reported result by Sun *et al.* showed that the  $R_{ct}$  of rGO is slightly lower than the  $R_{ct}$  value of rGO/Cu<sub>2</sub>O/CuO.<sup>48</sup> As can be seen in Table 2, the  $R_{ct}$  values were 4.13, 5.83, 6.28, and 9.46 Ohm for samples A, C, D, and E, respectively. The increase of the  $R_{ct}$  value for these samples was influenced by the increase of the average particle sizes of

Cu, Cu<sub>2</sub>O, and CuO. The increase in average size of the Cu, Cu<sub>2</sub>O, and CuO particles resulted in a longer diffusion path for electrons, which consequently inhibited electron transfer from the electrolyte to the electrode.<sup>49</sup>

Table 2 R<sub>ct</sub> and goodness of fit values of various rGO samples

Sample	R <sub>ct</sub> (Ohm)	Goodness of Fit
rGO	3.30	5.60 × 10 <sup>-03</sup>
Sample A	4.13	1.66 × 10 <sup>-03</sup>
Sample B	3.86	1.92 × 10 <sup>-03</sup>
Sample C	5.83	1.84 × 10 <sup>-03</sup>
Sample D	6.82	1.51 × 10 <sup>-03</sup>
Sample E	9.46	4.41 × 10 <sup>-04</sup>

Based on the structure, morphology, electrical conductivity, and EIS analysis results, we propose several possible explanations regarding the influence of Cu, Cu<sub>2</sub>O, and CuO presence in the rGO system on its electrical properties. In an attempt to explain the effect of Cu, Cu<sub>2</sub>O, and CuO interaction with rGO, an illustration of Cu, Cu<sub>2</sub>O, and CuO in rGO is presented in Fig. S12. For the role of Cu in rGO, we propose three possible explanations of Cu and rGO interaction. Firstly, from the Raman results, the role of Cu as n-doping in the interaction of Cu and rGO may serve as electron transfer to rGO sheets and thus electron transport from Cu to rGO may take place. Cu as n-doping in the interaction between Cu and rGO sheets is in agreement with previously reported results.<sup>41, 42</sup> Secondly, we assume that the copper may fill in or patch the vacancy or sp<sup>3</sup> carbon area (from the reduction of the carbonyl group (C=O) by hydrazine) in the rGO sheet, as shown in Fig. S12(a), top view. Hence, copper may serve as a bridge over the vacancy and resume electron mobility on the graphene surface. Thirdly, copper may serve as a spacer between layers, as shown in Fig. 12(a), side view. Copper as a spacer may ensure electron transport between rGO layers. The possibility of copper patching the vacancy and acting as a spacer are based on the interaction of Ag nanoparticles with rGO as reported by Han *et al.*,<sup>50</sup> who showed an example of Ag nanoparticles decorating the rGO surface and in between rGO layers.

A different role of the interaction of Cu<sub>2</sub>O and CuO with rGO was observed. Besides Cu, Cu<sub>2</sub>O and CuO were detected in samples **A** and **B**. Since sample **B** displayed the highest electrical conductivity and a lower R<sub>ct</sub> value, we may assume less agglomeration of Cu, Cu<sub>2</sub>O, and CuO particles in this sample. Thus, sample **B** follows illustration Fig. S12(a). As previously shown by the SEM results, the agglomeration of Cu, Cu<sub>2</sub>O, and CuO particles was observed in sample **A**, which led to a decrease in electrical conductivity and an increase in R<sub>ct</sub> value. By adding a copper concentration of 2 and 3 wt% in the mixture of CuO and GO (samples **C** and **D**), the reduction process resulted in the formation of Cu<sub>2</sub>O and bigger particles of Cu and a mixture of Cu and Cu<sub>2</sub>O, as shown in Fig. S12(b). A similar result was observed for sample **E**. Increasing the concentration to 5 wt% led to more Cu<sub>2</sub>O formation and

remaining CuO, which consequently increased the particle sizes of the Cu<sub>2</sub>O and CuO due to agglomeration, as depicted in Fig S12(c). Moreover, the Cu<sub>2</sub>O and CuO showed electrical resistivity,<sup>44</sup> and thus samples **A**, **C**, **D**, and **E** displayed lower electrical conductivity and higher R<sub>ct</sub> values compared to sample **B**.

## Conclusions

Samples of rGO and rGO with copper addition were successfully synthesized via in situ chemical exfoliation using a microwave-assisted method. Structural and morphological characterizations of the samples by ATR-FTIR, XRD, Raman, EDX, and SEM confirmed the formation of rGO and the presence of Cu, Cu<sub>2</sub>O, and/or CuO. The copper precursor concentration added to the mixture of CuO and GO ≤ 1 wt% during reduction resulted in the formation of rGO and Cu, which led to further reduction of rGO and formation of CuO. The annealing treatment (300 °C for 45 minutes) of sample **B** resulted in further improvement of the electrical conductivity of the rGO, yielding the highest electrical conductivity of 24.85 S/cm. The presence of a small concentration of Cu and CuO in the rGO did not influence the R<sub>ct</sub> value of the rGO. However, the addition of copper precursor with concentration ≥ 2 wt% in the mixture of CuO and GO led to the formation of rGO, Cu, Cu<sub>2</sub>O, and/or remaining CuO. The presence of Cu<sub>2</sub>O and CuO in the rGO caused a decrease of the electrical conductivity and electrochemical properties. Furthermore, increasing the concentration of copper precursor caused more agglomeration of copper particles. Therefore, the electrical conductivity further decreased and the R<sub>ct</sub> values of the materials increased.

## Conflicts of interest

"There are no conflicts to declare".

## Acknowledgments

This work was supported partially by Penelitian Unggulan Perguruan Tinggi (PUPT) 2016, Ministry of Education, Research, and Technology, Republic of Indonesia. We gratefully acknowledge the support from the United States Agency International Development (USAID) through the Sustainable Higher Education Research Alliances (SHERA) program. We would like to thank Dr. Arramel and Ms. Tan Wei Ling (National University of Singapore) for their kind assistance in conducting the Raman measurements. We would like to thank Dr. Isdiriyani Nuridin (Chemical Engineering Department, ITB) for her kind assistance in conducting the EIS measurements. E. Stavila would like to thank the Insentif Postdoc Program, ITB, for the funding support.

## References

1. C. Sarkar and S. K. Dolui, *RSC Adv.*, 2015, **5**, 60763-60769.

2. K. S. Novoselov, A. K. Geim, S. V. Morozov, D. Jiang, Y. Zhang, S. V. Dubonos, I. V. Grigorieva and A. A. Firsov, *Science*, 2004, **306**, 666.
3. N. O. Weiss, H. Zhou, L. Liao, Y. Liu, S. Jiang, Y. Huang and X. Duan, *Adv. Mater.*, 2012, **24**, 5782-5825.
4. Z.-S. Wu, G. Zhou, L.-C. Yin, W. Ren, F. Li and H.-M. Cheng, *Nano Energy*, 2012, **1**, 107-131.
5. K. S. Novoselov, V. I. Falko, L. Colombo, P. R. Gellert, M. G. Schwab and K. Kim, *Nature*, 2012, **490**, 192-200.
6. R. Raccichini, A. Varzi, S. Passerini and B. Scrosati, *Nat. Mater.*, 2015, **14**, 271-279.
7. B. Bashir, W. Shaheen, M. Asghar, M. F. Warsi, M. A. Khan, S. Haider, I. Shakir and M. Shahid, *J. Alloys Compd.*, 2017, **695**, 881-887.
8. M. Pumera, *Chem. Rec.*, 2009, **9**, 211-223.
9. P. Bollella, G. Fusco, C. Tortolini, G. Sanzò, G. Favero, L. Gorton and R. Antiochia, *Biosens. Bioelectron.*, 2017, **89**, 152-166.
10. J. Luo, S. Jiang, H. Zhang, J. Jiang and X. Liu, *Anal. Chim. Acta*, 2012, **709**, 47-53.
11. Y. M. Lin, C. Dimitrakopoulos, K. A. Jenkins, D. B. Farmer, H. Y. Chiu, A. Grill and P. Avouris, *Science*, 2010, **327**, 662.
12. M. B. Gawande, A. Goswami, F.-X. Felpin, T. Asefa, X. Huang, R. Silva, X. Zou, R. Zboril and R. S. Varma, *Chem. Rev.*, 2016, **116**, 3722-3811.
13. B. Wang, J. He, F. Liu and L. Ding, *J. Alloys Compd.*, 2017, **693**, 902-908.
14. B. Wang, X.-L. Wu, C.-Y. Shu, Y.-G. Guo and C.-R. Wang, *J. Mater. Chem.*, 2010, **20**, 10661-10664.
15. C.-T. Hsieh, W.-H. Lin, Y.-F. Chen, D.-Y. Tzou, P.-Q. Chen and R.-S. Juang, *J. Taiwan Inst. Chem. Eng.*, 2017, **71**, 77-83.
16. X. Dong, K. Wang, C. Zhao, X. Qian, S. Chen, Z. Li, H. Liu and S. Dou, *J. Alloys Compd.*, 2014, **586**, 745-753.
17. M. Khan, M. N. Tahir, S. F. Adil, H. U. Khan, M. R. H. Siddiqui, A. A. Al-warthan and W. Tremel, *J. Mater. Chem. A*, 2015, **3**, 18753-18808.
18. Y. Areerob, K.-Y. Cho and W.-C. Oh, *New J. Chem.*, 2017, DOI: 10.1039/c7nj01782k.
19. P. Borthakur, P. K. Boruah, G. Darabdhara, P. Sengupta, M. R. Das, A. I. Boronin, L. S. Kibis, M. N. Kozlova and V. E. Fedorov, *J. Environ. Chem. Eng.*, 2016, **4**.
20. N. Garino, A. Sacco, M. Castellino, J. A. Muñoz-Tabares, M. Armandi, A. Chiodoni and C. F. Pirri, *ChemistrySelect*, 2016, **1**, 3640-3646.
21. S. Gayathri, M. Kottaisamy and V. Ramakrishnan, *AIP Adv.*, 2015, **5**.
22. A. M. Noor, P. Rameshkumar, N. Yusoff, H. N. Ming and M. S. Sajab, *Ceram. Int.*, 2016, **42**, 18813-18820.
23. K. C. Hsu and D. H. Chen, *Nanoscale Res. Lett.*, 2014, **9**, 1-9.
24. H. Wadhwa, D. Kumar, S. Mahendia and S. Kumar, *Mater. Chem. Phys.*, 2017, **194**, 274-282.
25. C. Lamiel, V. H. Nguyen, C. Roh, C. Kang and J. J. Shim, *Electrochim. Acta*, 2016, **210**, 240-250.
26. J. Lim, J. Gim, J. Song, D. T. Nguyen, S. Kim, J. Jo, V. Mathew and J. Kim, *J. Power Sources*, 2016, **304**, 354-359.
27. A. H. Mady, M. L. Baynosa, D. Tuma and J. J. Shim, *Appl. Catal. B: Environ.*, 2017, **203**, 416-427.
28. X. Xu, J. Shen, N. Li and M. Ye, *J. Alloys Compd.*, 2014, **616**, 58-65.
29. F. Iskandar, U. Hikmah, E. Stavila and A. H. Aimon, *RSC Adv.*, 2017, **7**, 52391-52397.
30. H. Miftahul, A. F. Hafizh, F. Rohman, H. A. Akfany and I. Ferry, *Mater. Res. Express*, 2017, **4**, 064001.
31. D. W. Lee, L. De Los Santos V, J. W. Seo, L. L. Felix, A. Bustamante D, J. M. Cole and C. H. W. Barnes, *J. Phys. Chem. B*, 2010, **114**, 5723-5728.
32. Z. Ji, G. Zhu, X. Shen, H. Zhou, C. Wu and M. Wang, *New J. Chem.*, 2012, **36**, 1774-1780.
33. Y. T. Prabhu, K. Venkateswara Rao, V. Sesha Sai and T. Pavani, *J. Saudi Chem. Soc.*, 2017, **21**, 180-185.
34. S. M. Pawar, J. Kim, A. I. Inamdar, H. Woo, Y. Jo, B. S. Pawar, S. Cho, H. Kim and H. Im, *Sci. Rep.*, 2016, **6**, 21310.
35. W. Li and Y. J. Yang, *J. Solid State Electr.*, 2014, **18**, 1621-1626.
36. D. Voiry, J. Yang, J. Kupferberg, R. Fullon, C. Lee, H. Y. Jeong, H. S. Shin and M. Chhowalla, *Science*, 2016, **353**, 1413.
37. I. Childres, L. A. Jauregui, W. Park, H. Cao and Y. P. Chena, *Raman Spectroscopy of Graphene and Related Materials*, 2013.
38. S. Abdolhosseinzadeh, H. Asgharzadeh and H. Seop Kim, *Sci. Rep.*, 2015, **5**, 10160.
39. S. Stankovich, D. A. Dikin, R. D. Piner, K. A. Kohlhaas, A. Kleinhammes, Y. Jia, Y. Wu, S. T. Nguyen and R. S. Ruoff, *Carbon*, 2007, **45**, 1558-1565.
40. V. C. Tung, M. J. Allen, Y. Yang and R. B. Kaner, *Nat. Nanotech.*, 2008, **4**, 25.
41. J. Lee, K. S. Novoselov and H. S. Shin, *ACS Nano*, 2011, **5**, 608-612.
42. G. Giovannetti, P. A. Khomyakov, G. Brocks, V. M. Karpan, J. van den Brink and P. J. Kelly, *Phys. Rev. Lett.*, 2008, **101**, 026803.
43. D. Parobek, G. Shenoy, F. Zhou, Z. Peng, M. Ward and H. Liu, *J. Chem. Educ.*, 2016, **93**, 1798-1803.
44. L. De Los Santos Valladares, D. H. Salinas, A. B. Dominguez, D. A. Najarro, S. I. Khondaker, T. Mitrelias, C. H. W. Barnes, J. A. Aguiar and Y. Majima, *Thin Solid Films*, 2012, **520**, 6368-6374.
45. X. Gao, J. Jang and S. Nagase, *J. Phys. Chem. C*, 2010, **114**, 832-842.
46. R. Larciprete, S. Fabris, T. Sun, P. Lacovig, A. Baraldi and S. Lizzit, *J. Am. Chem. Soc.*, 2011, **133**, 17315-17321.
47. Gamry, Equivalent Circuit Modeling Using the Gamry EIS300 Electrochemical Impedance Spectroscopy Software, <https://www.gamry.com/application-notes/EIS/equivalent-circuit-modeling-using-the-gamry-eis300-electrochemical-impedance-spectroscopy-software/>, (accessed 30 November, 2017).
48. L. Sun, Q. Deng, Y. Li, L. Deng, Y. Wang, X. Ren and P. Zhang, *Electrochim. Acta*, 2016, **222**, 1650-1659.
49. T. V. S. L. Satyavani, B. Ramya Kiran, V. Rajesh Kumar, A. Srinivas Kumar and S. V. Naidu, *Eng. Sci. Technol. Int J.*, 2016, **19**, 40-44.
50. L. Han, C.-M. Liu, S.-L. Dong, C.-X. Du, X.-Y. Zhang, L.-H. Li and Y. Wei, *Biosens. Bioelectron.*, 2017, **87**, 466-472.

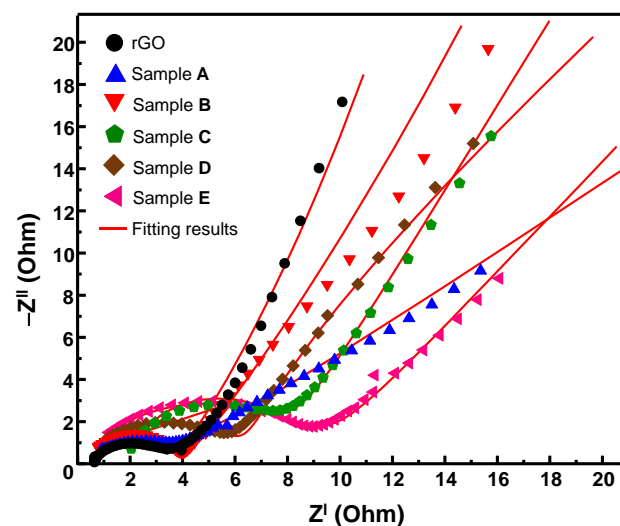
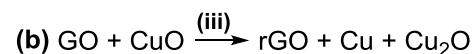
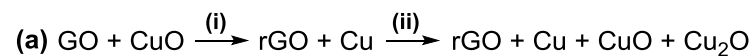
# The Influence of Copper Addition on Electrical Conductivity and Charge Transfer Resistance of Reduced Graphene Oxide (rGO)

Ferry Iskandar,<sup>\*a,b,c</sup> Oktaviardi Bityasmawan Abdillah,<sup>a</sup> Erythrina Stavila,<sup>c</sup> and Akfiny Hasdi Aimon<sup>a,b</sup>

<sup>a</sup> Department of Physics, Faculty of Mathematics and Natural Sciences, Institut Teknologi Bandung, Jl. Ganesha 10 Bandung, 40132, Indonesia. E-mail: ferry@fi.itb.ac.id

<sup>b</sup> National Center for Sustainable Transportation Technology (NCSTT), Institut Teknologi Bandung, Jl. Ganesha 10 Bandung, 40132, Indonesia

<sup>c</sup> Research Center for Nanosciences and Nanotechnology (RCNN), Institut Teknologi Bandung, Jl. Ganesha 10, Bandung, 40132, Indonesia



The possible explanations on how copper, CuO, or Cu<sub>2</sub>O existence influence the electrical conductivity and electrochemical properties of rGO.